Bifunctional Catalyst MoS_x@H-Beta for Highly Selective Conversion of CO_2 to C_{2-6} Hydrocarbons

Taotao Zhao[1†], Chenyang Shen[1†], Yuchi Liu[1], Gui Liu[1], Xiaofeng Qian[1], Qiang He[1], Feifei Mei[1], Yu He[1], Xiangke Guo[1], Nianhua Xue[1], Xi Liu[2] and Weiping Ding[1]**

[1] Key Lab of Mesoscopic Chemistry, School of Chemistry and Chemical Engineering, Nanjing University, Nanjing 210023, China

[2] School of Chemistry and Chemical, In-situ Centre for Physical Sciences, Frontiers Science Centre for Transformative Molecules, Shanghai Jiao Tong University, Shanghai, 200240, P. R. China

[†] These authors contributed equally.

*Correspondence author: dingwp@nju.edu.cn; nianhua@nju.edu.cn

Supporting Information includes:

Chemical reagents

Catalyst Characterization

Catalyst Evaluation

DFT simulations

Figures S1-S16

Tables S1-S4

Chemical reagents

H-Beta zeolite was purchased from Nankai University Catalyst Co., Ltd. Both MoO_3 (99.5 wt.%) and MoS_2 (99.5 wt.%) were purchased from Aladdin Reagent Co., Ltd. Sulfur powder (99.9 wt.%) was purchased from Sigma-Aldrich Reagent Co., Ltd. NaOH (AR 95 wt.%) was purchased from Shanghai macklin biochemical Co., Ltd. Ethanol (AR) was purchased from Sinopharm Group Chemical Reagent Co., Ltd.

Catalyst Characterization

X-ray diffraction (XRD) patterns were recorded on an X'pert PAN analytical diffractometer (Cu Ka radiation, 40 kV, 40 mA) from 5 to 50° in 2θ. Scanning electron microscopy (SEM) images were performed on the S-4800 field emission SEM with accelerating voltage of 5 kV. High Resolution Transmission Electron Microscope (HR-TEM) were executed on the High Throughput Elctron Microscope JEM-2800 at accelerating voltage of 200 kV. Probe Corrected Scanning Transmission Electron Microscope (STEM) were executed on the ThermoFisher ThemisZ at accelerating voltage of 300 kV with High Angle Annual Dark Field (HAADF) and Integrated Differential Phase Contrast (iDPC) two kind detection modes, respectively. The iDPC imaging technology could image light atoms under low irradiation dose and perform non-destructive imaging of zeolite channel structure. The HAADF imaging technology could make heavy atoms display higher brightness and directly image zeolite and channel fillers. The Mo k-edge (20000 eV) X-ray absorption fine structure (XAFS) spectroscopy of samples were investigated on BL14W1 beamline of Shanghai Synchrotron Radiation Facility. X-ray photoelectron spectroscopy (XPS) measurements were performed on a ThermoFisher ThemisZ Escalab XPS system equipped with Al Kα (hv = 1486.6 eV) X-ray as exciting source. The content of Mo in catalyst was measured via inductively coupled plasma-optical emission spectrometer (ICP-OES, Agilent 725-ES). The specific Brunauer-Emmett-Teller (BET) surfaces were analyzed with a Micromeritics ASAP 2010 analyzer at liquid nitrogen (77 K) environment, catalyst was degassed at 300 °C for 4 hours under 10^{-3} Torr vacuum before the test. The H-D exchange spectra of samples were obtained by PFEIFFER mass spectrometer. The CO_2-TPD patterns of samples were monitored by TP-5076 dynamic adsorption instrument.

Catalytic Evaluation

CO_2 hydrogenation reaction was performed on the fixed-bed reactor equipped with gas chromatograph (GC-9860). In typical procedure, the powder catalyst was prepared into granule (20-40 mesh) prior to testing. 0.3 g catalyst granule was filled in the U-shaped stainless-steel tube with 4 mm inner diameter. In order to avoid interference of air and conveniently calculate CO_2 conversion in the later stage, the reaction gas (23% CO_2, 69% H_2, and 8% Ar) was introduced into the continuous-flow reactor for a stretch under room temperature and reaction pressure. Finally, the effects of temperature, pressure and space velocity on the catalyst for CO_2 hydrogenation reaction were investigated. The reaction off-gas maintained at 130 °C was sent to the gas chromatograph (GC-9860) equipped with FID and TCD detector for online analysis. The Plot Q capillary column was connected in front of FID detector to detect organic products, and TCD detector was connected to the PN packed column to detect CO_2, Ar and CO gas, respectively. All substances were qualitatively determined by comparing the retention times with the standards. Catalytic data were calculated using argon (Ar) as internal standard.

$$CO_2\ \text{conversion} = \frac{CO_2^{in} - CO_2^{out}}{CO_2^{in}} \times 100\%$$

* MERGEFORMAT (1)

$$CO\ \text{selectivity} = \frac{CO^{out}}{CO_2^{in} - CO_2^{out}} \times 100\%$$

* MERGEFORMAT (2)

C_x hydrocarbons and CH_3OH selectivity in organic products were obtained in equation (3) and (4), respectively.

$$C_x\ \text{selectivity} = \frac{f_{C_x} \cdot A_{C_x}}{f_{CH_3OH} \cdot A_{CH_3OH} + \sum_{i=1}^{n} f_{C_i} \cdot A_{C_i}} \times 100\%$$

* MERGEFORMAT (3)

$$CH_3OH\ \text{selectivity} = \frac{f_{CH_3OH} \cdot A_{CH_3OH}}{f_{CH_3OH} \cdot A_{CH_3OH} + \sum_{i=1}^{n} f_{C_i} \cdot A_{C_i}} \times 100\%$$

* MERGEFORMAT (4)

Where COin 2, COout 2 and CO^{out} represented mass of CO_2 and CO at the inlet and outlet, respectively. Letter A and f represented peak area and quality correction factor, respectively.

DFT simulations

Computational methods: All DFT simulations were conducted using the Vienna Ab initio Simulation Package (VASP 5.4.4)[1, 2], employing the generalized gradient approximation in the Perdew-Burker-Ernzerhof (PBE) exchange-correlation functional[3]. The core electrons were described with projector augmented-wave pseudopotentials (PAW)[4] and the valence electrons were expanded from a plane-wave basis set with a cutoff energy of 400 eV[5]. A Γ-centered *k*-point grid of 1×1×1 was selected for the sampling of the Brillouin zone. The convergences of energy and gradient were set as 10^{-5} and 0.03 eV $Å^{-1}$, respectively. The adsorption energy was defined as the energy difference between the initial state (IS) and final state (FS), while the activation barrier was calculated based on the energy difference between the initial state and transition state (TS). All transition states were located based on the climbing-image nudged elastic band (CI-NEB)[6] combined with the improved dimer method (IDM)[7], and finally confirmed via frequency analysis. The atomic charges were computed via the Bader charge analysis[8].

Computational model: The pristine H-Beta zeolite was constructed based on a repeated unit with the lattice constant of 12.66 Å × 12.66 Å × 26.40 Å (Fig. 7(a)). According to the experimental Si/Al ratio of 20, some of Si atoms in the zeolite framework were selectively substituted by Al atoms. Herein, the most symbolic 12-membered ring (12-MR) of H-Beta was chosen for hosting the Mo_xS_y species. In consideration of the ring size, a classic Mo_3S_4 model (Fig. 7(b)) was adopted with Mo-Mo and Mo-S length of 2.59 Å and ~2.32 Å, respectively. As for the structural optimization, the O atoms of the 12-MR were all saturated with H atoms and the obtained -OHs were fixed in view of the rigid frame structure of H-Beta zeolite. After encapsulated by the cage of H-Beta zeolite, as shown in Fig. 7(c), Mo_3S_4 cluster remained relatively stable and formed two chemical bonds with the O atoms from the 12-MR, leaving the Mo-O bond lengths of 2.02 Å and 2.26 Å, respectively.

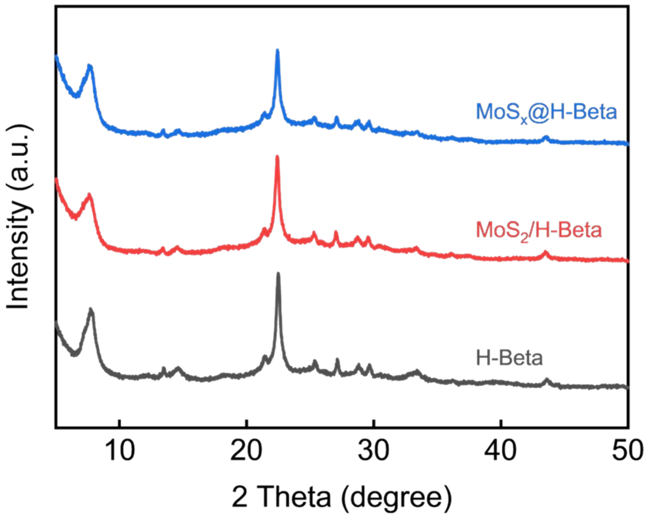

Fig. S1 XRD patterns of commercial H-Beta zeolite, MoS$_2$/H-Beta and MoS$_x$@H-Beta.

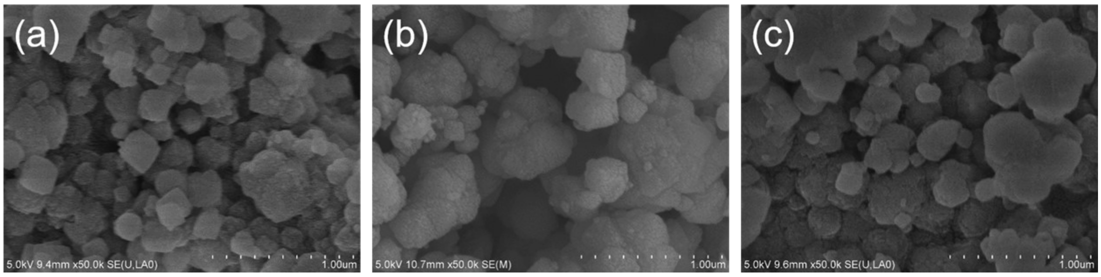

Fig. S2 SEM images of H-Beta (a), MoS$_2$/H-Beta (b) and MoS$_x$@H-Beta (c).

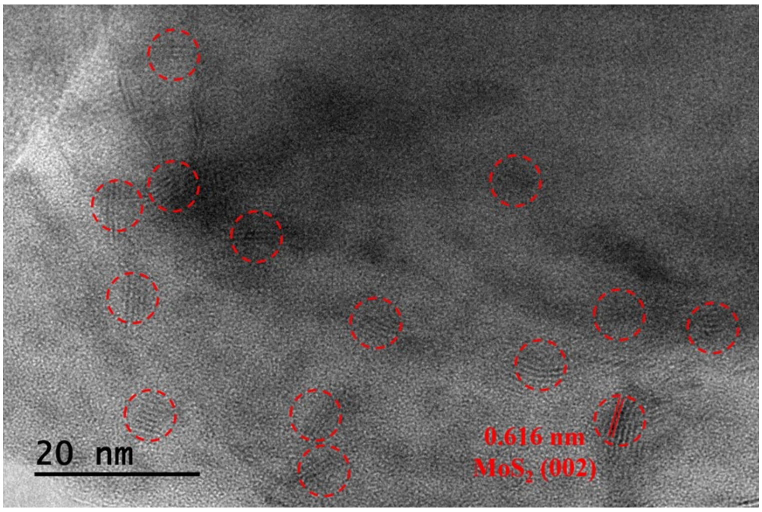

Fig. S3 HR-TEM image of MoS$_2$/H-Beta.

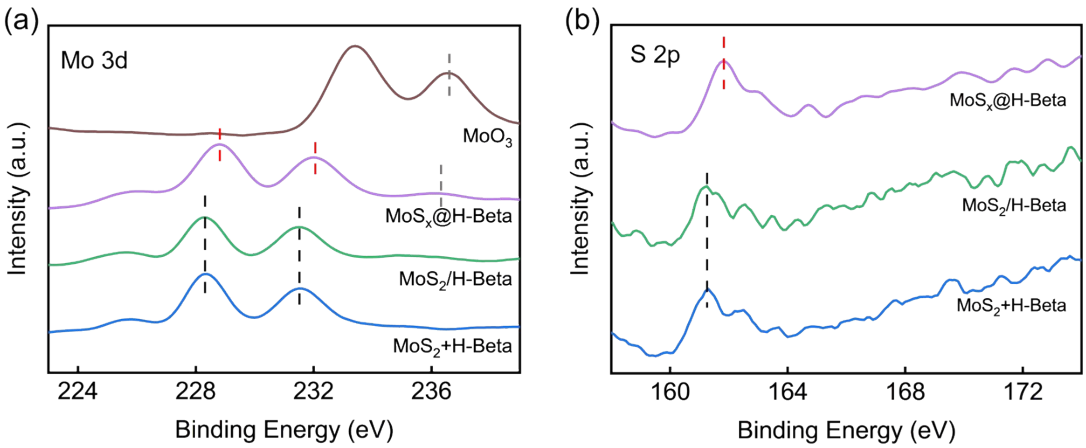

Fig. S4 The XPS spectra of MoS_2+H-Beta, MoS_2/H-Beta, MoS_x@H-Beta and MoO_3: (a) Mo 3d and (b) S 2p.

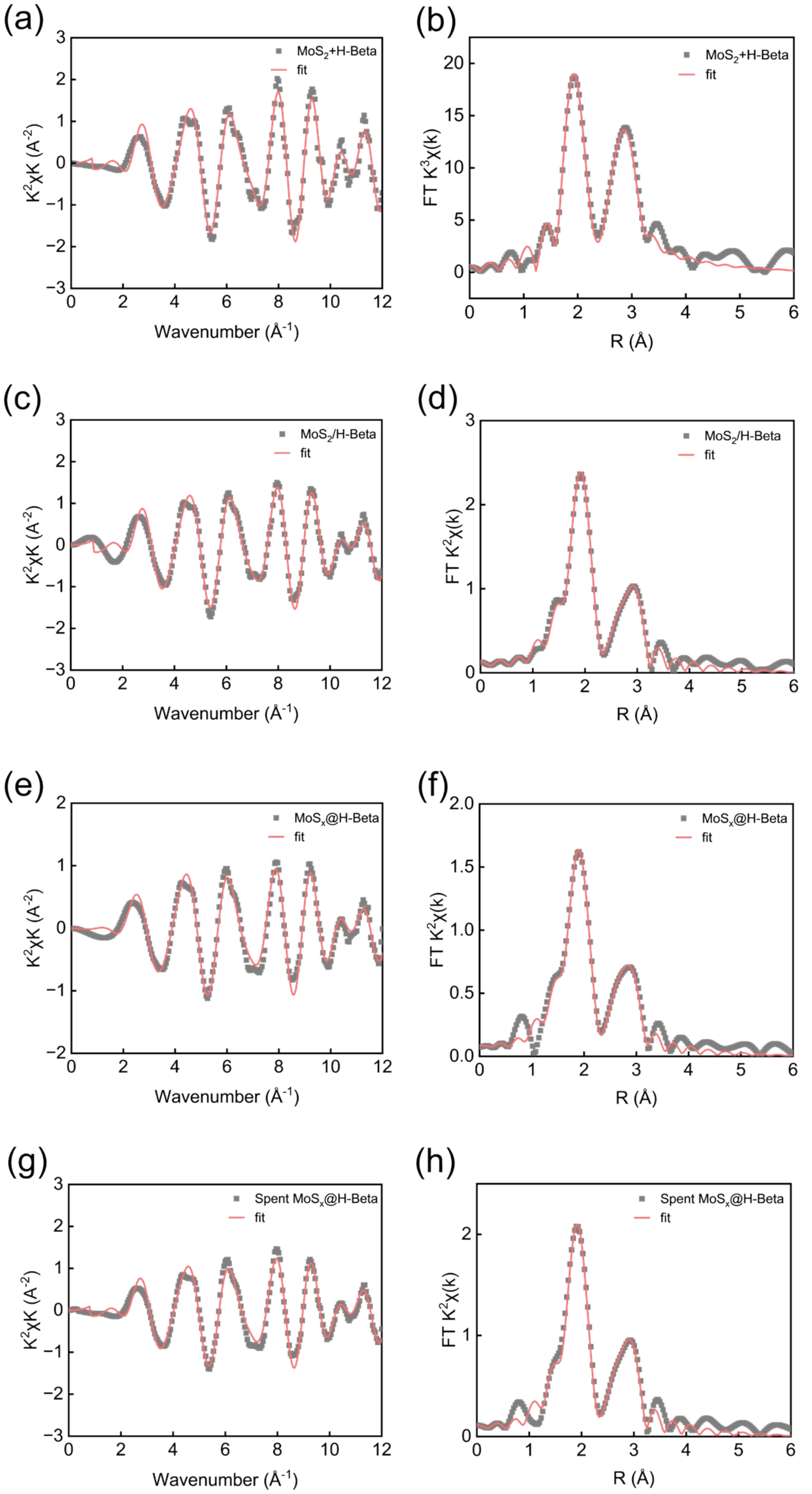

Fig. S5 Results of Mo K-edge EXAFS data fitting: (a, b) MoS_2+H-Beta, (c, d) MoS_2/H-Beta, (e, f) MoS_x@H-Beta and (g, h) spent MoS_x@H-Beta

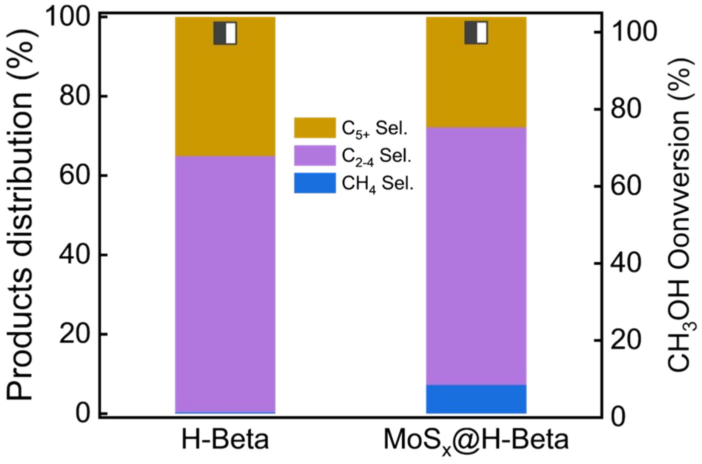

Fig. S6 Evaluation of catalytic activity of commercial H-Beta zeolite and MoS$_x$@H-Beta for methanol to hydrocarbons reaction under reaction condition: 350 ºC, atmospheric pressure and 0.2 mL$_{MeOH}$ g$^{-1}_{cat}$ h^{-1}.

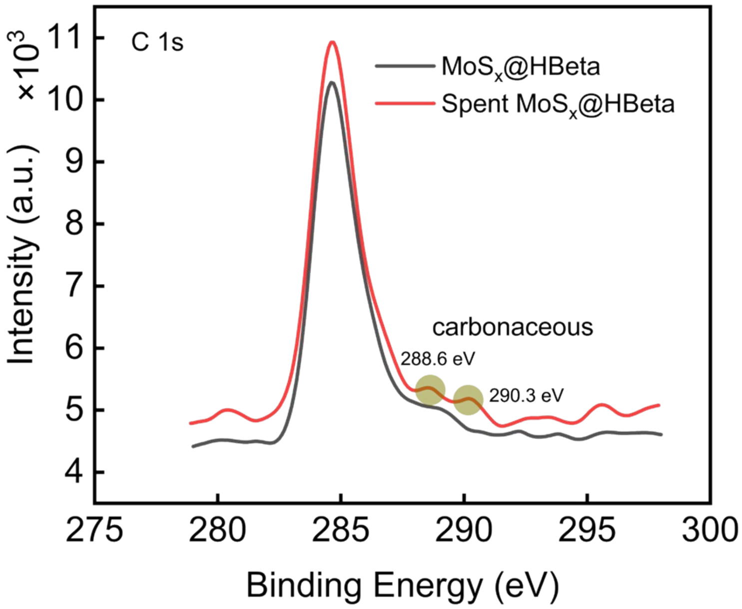

Fig. S7 The C 1s XPS spectra of MoS$_x$@H-Beta and spent MoS$_x$@H-Beta[9, 10].

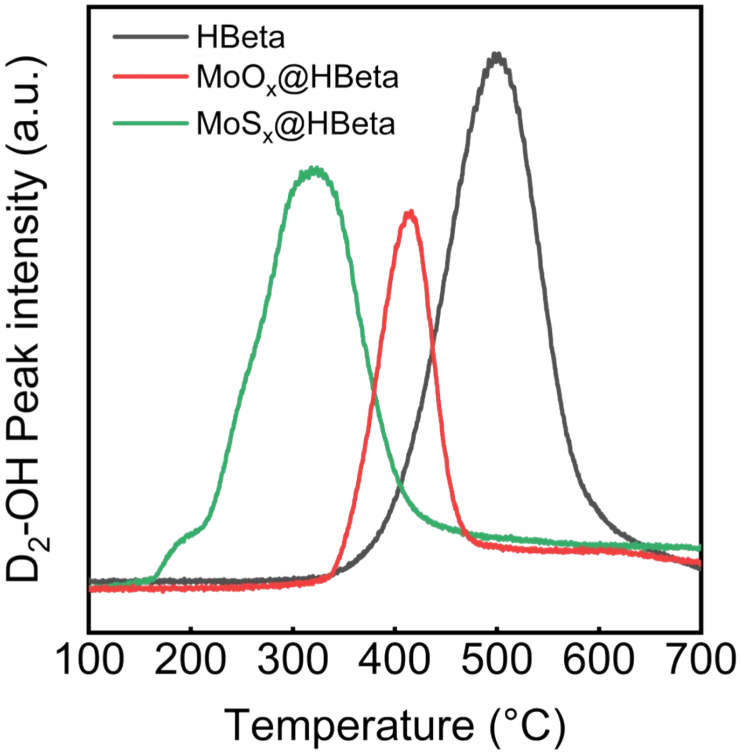

Fig. S8 The D_2-OH exchange of H-Beta, MoO_x@H-Beta and MoS_x@H-Beta.

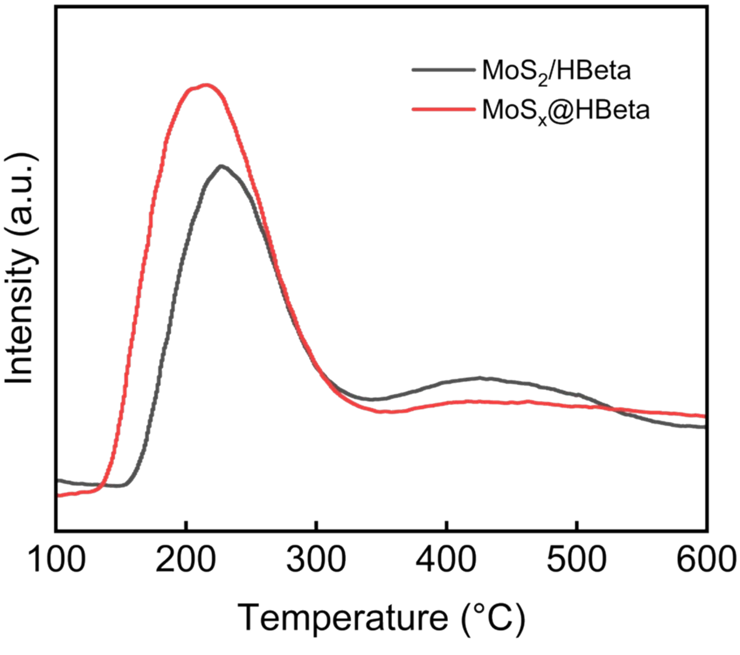

Fig. S9 The CO_2-TPD spectrum of MoS_2/H-Beta and MoS_x@H-Beta.

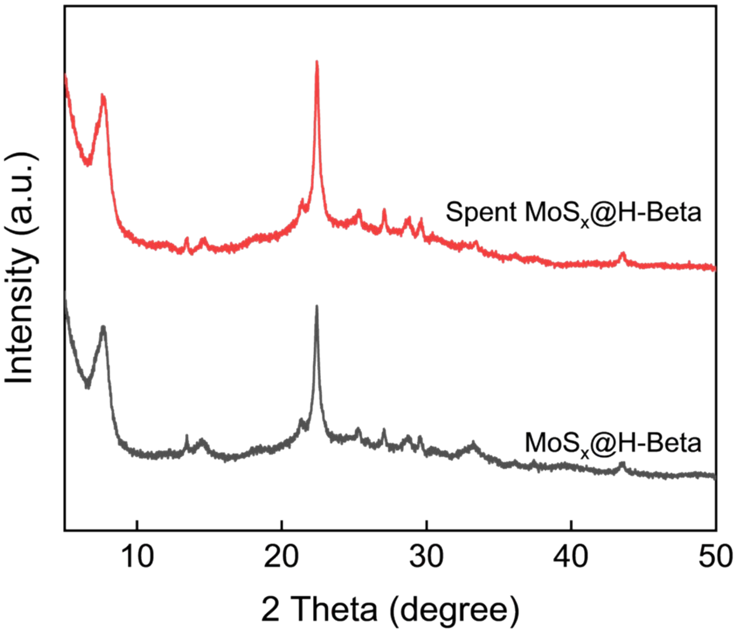

Fig. S10 XRD patterns of MoS$_x$@H-Beta and spent MoS$_x$@H-Beta.

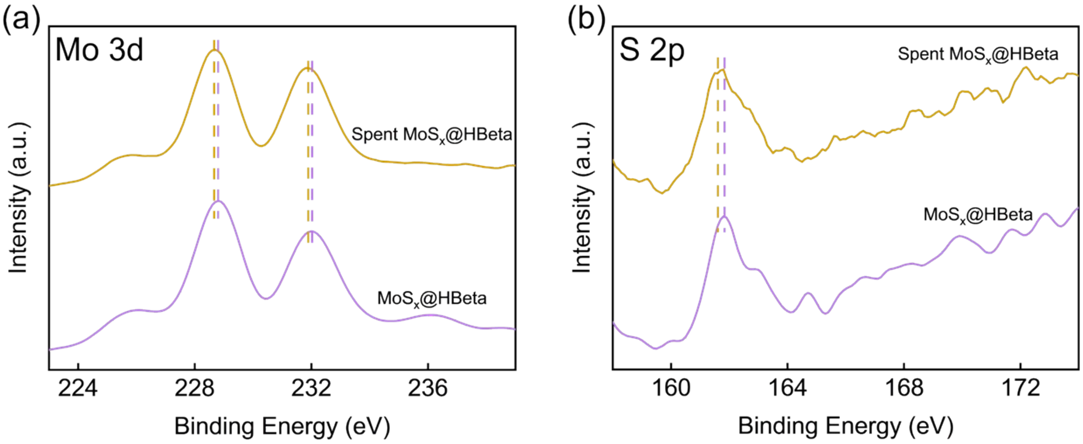

Fig. S11 The XPS spectra of MoS$_x$@H-Beta and spent MoS$_x$@H-Beta: (a) Mo 3d and (b) S 2p.

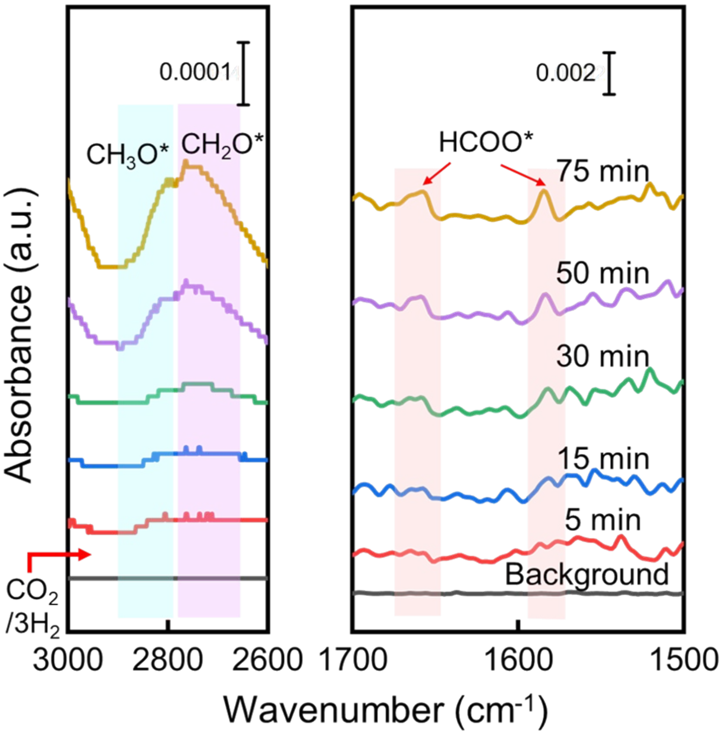

Fig. S12 Operando DRIFT spectra of MoS_x@Na-Beta catalyst under continuous reaction of CO_2 hydrogenation ($CO_2/3H_2$, 0.1 MPa, 200 °C).

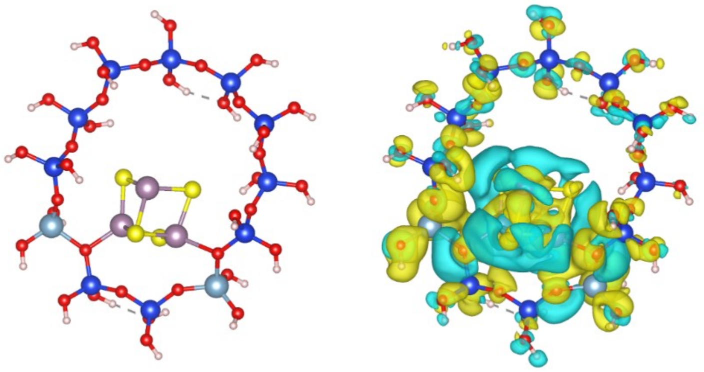

Fig. S13 The charge difference density over Mo_3S_4@H-Beta. The yellow and blue contours represent the electron density accumulations and depressions, respectively.

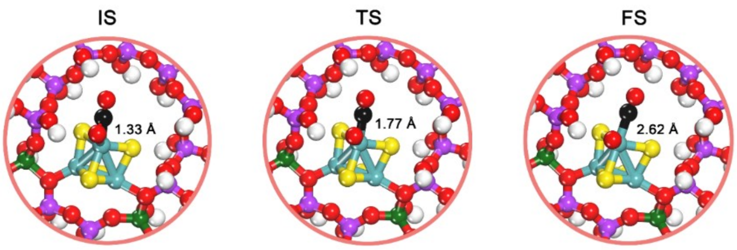

Fig. S14 The initial state, transition state and final state of elementary step [$CO_2^* \rightarrow CO^* + O^*$]

over the Mo_3S_4@H-Beta. Color mode: Si (violet), Al (green), O (red), Mo (cyan), S (yellow), C (black), and H (white).

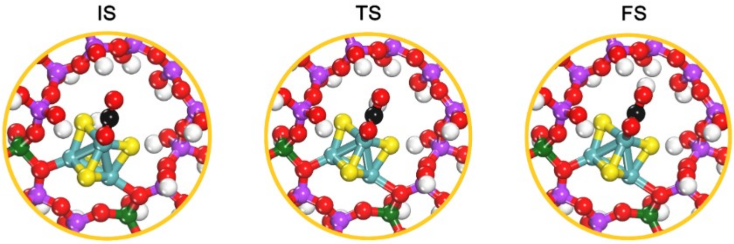

Fig. S15 The initial state, transition state and final state of elementary step [CO_2*+H*→COOH*] over the Mo_3S_4@H-Beta. Color mode: Si (violet), Al (green), O (red), Mo (cyan), S (yellow), C (black), and H (white).

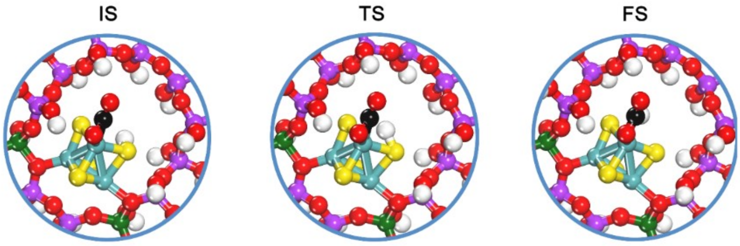

Fig. S16 The initial state, transition state and final state of elementary step [CO_2*+H*→HCOO*] over the Mo_3S_4@H-Beta. Color mode: Si (violet), Al (green), O (red), Mo (cyan), S (yellow), C (black), and H (white).

Table S1 Mo content (wt. %) and BET specific surface area of various samples.

Samples·	**Mo (wt. %)**	**BET specific surface area (m^2/g)**
H-Beta	None	629
MoS_2/H-Beta	5.32	546
MoS_x@H-Beta	5.51	444

Table S2 The mole ratio of sulfur to molybdenum in commercial MoS_2+H-Beta, MoS_2/H-Beta, MoS_x@H-Beta, and Spent MoS_x@H-Beta obtained from XPS techniques.

Samples	**Mole ratio of S/Mo**
MoS_2+H-Beta	1.90
MoS_2/H-Beta	1.87
MoS_x@H-Beta	1.13
Spent MoS_x@H-Beta	1.10

Table S3 Mo k-edge EXAFS data for the Mo based catalysts[a]

Samples	Scattered	Shell	R (Å)[b]	CN[c]	σ^2 ($Å^2$)[d]	e0
MoS_2+H-Beta	Mo	Mo-S	2.41	6	0.0018	2.5
		Mo-S-Mo	3.16	6	0.0022	-1.0
MoS_2/H-Beta	Mo	Mo-S	2.41	4.9±0.3	0.0023	2.8
		Mo-S-Mo	3.16	3.5±0.8	0.0023	0.2
MoS_x@H-Beta	Mo	Mo-S	2.41	3.9±0.4	0.0019	-2.0
		Mo-S-Mo	3.15	2.9±0.8	0.0018	-6.1
Spent MoS_x@H-Btea	Mo	Mo-S	2.41	4.1±0.4	0.0023	2.6
		Mo-S-Mo	3.16	3.1±1.0	0.0023	-0.2

a: The R-factor of fitting in MoS_2/H-Beta, MoS_x@H-Beta and Spent MoS_x@H-Btea were 0.004, 0.004 and 0.008, respectively; **b**: Bond length; **c**: Coordination number; **d**: Debye-Waller factor.

Table S4 Atomic Bader charge analysis results (in |e|) for Mo_3S_4 cluster and Mo_3S_4@H-Beta

	Mo_1	**Mo_2**	**Mo_3**	**S_1**	**S_2**	**S_3**	**S_4**	**Total**
Mo_3S_4	0.88	0.92	0.86	-0.56	-0.72	-0.65	-0.73	0
Mo_3S_4@H-Beta	1.26	0.95	1.19	-0.56	-0.40	-0.47	-0.45	+1.52

References

1 G. Kresse and J. Furthmüller, *Phys. Rev. B,* 1996, **54**, 11169-11186.

2 G. Kresse and J. Furthmüller, *Comput. Mater. Sci.,* 1996, **6**, 15-50.

3 J. Perdew, K. Burke and M. Ernzerhof, *Phys. Rev. Lett.,* 1996, **77**, 3865-3868.

4 P. Blöchl, *Phys. Rev. B,* 1994, **50**, 17953-17979.

5 G. Liu, P. Liu, D. Meng, T. Zhao, X. Qian, Q. He, X. Guo, J. Qi, L. Peng, N. Xue, Y. Zhu, J. Ma, Q. Wang, X. Liu, L. Chen and W. Ding, *Nat. Commun.,* 2023, **14**, 513-513.

6 G. Henkelman and H. Jónsson, *J. Chem. Phys.,* 2000, **113**, 9978-9985.

7 G. Henkelman and H. Jónsson, *J. Chem. Phys.,* 1999, **111**, 7010-7022.

8 R. Bader, *Chem. Rev.,* 1991, **91**, 893-928.

9 D. Briggs and G. Beamson, *Anal. Chem.,* 1992, **64,** 1729-1736.

10 G. Barth, R. Linder and C. Bryson, *Surf. Interfaces,* 1988, **11,** 307-311.